Applied Catalysis B: Environmental 310 (2022) 121335

Contents lists available at ScienceDirect

Applied Catalysis B: Environmental

journal homepage: www.elsevier.com/locate/apcatb

2D covalent organic frameworks for photosynthesis of α-trifluoromethylated ketones from aromatic alkenes

Ziping Li [a,1], Jia-ao Wang [b,1], Si Ma [a], Zhenwei Zhang [a], Yongfeng Zhi [a], Fuchun Zhang [d], Hong Xia [c], Graeme Henkelman [b,*], Xiaoming Liu [a,*]

[a] College of Chemistry, Electron Microscopy Center, Jilin University, Changchun 130012, PR China
[b] Department of Chemistry and the Oden Institute for Computational Engineering and Sciences, The University of Texas at Austin, Austin, TX 78712-0165, USA
[c] State Key Laboratory on Integrated Optoelectronics, College of Electronic Science and Technology, Jilin University, Changchun 130012, PR China
[d] School of Physics and Electronic Information, Yan'an University, Yan'an 716000, PR China

ARTICLE INFO

Keywords:
Covalent organic frameworks
Photocatalysis
α-Trifluoromethylated ketones
Trifluoromethylation
Visible light

ABSTRACT

Photoactive two-dimensional covalent organic frameworks (2D-COFs) have recently emerged as a promising platform for efficient solar to chemical energy conversion. The photosynthesis of α-trifluoromethylated ketones, which is an important access to various fluorine-containing compounds, is rarely reported in heterogeneous photocatalytic systems. Herein, we report two 2D-COFs constructed from the electron-deficient triazine and electron-rich benzotrithiophene units with imine and amide linkages for the photosynthesis of α-trifluoromethylated ketones. The novel triazine-based COFs showed good activity, broad substrate flexibility and recyclability under visible-light irradiation, which is much superior to the classical pyrene-based COFs. Density functional theory calculations revealed that the triazine-based COFs have intrinsically lower carrier recombination tendency and can produce more intermediates •CF_3, resulting in higher catalytic efficiency. This research will contribute to the rational design of photoactive COFs and facilitate the development of fluorine chemistry.

1. Introduction

Organic compounds containing trifluoromethyl (CF_3) group are extensively prevalent in pharmaceuticals, functional materials and agrochemicals, because the CF_3 group can profoundly affect the physical, chemical and biological characters of parent molecules [1]. Over the past decades, the preparation of α-trifluoromethylated ketone compounds, that are valuable building blocks for the construction of a wide variety of fluorinated products [2], has become a preferential research topic in synthetic chemistry. Generally, they can be achieved through electrophilic or radical trifluoromethylation of enolates and silyl enol ethers [3–5]. And the nucleophilic trifluoromethylation process of α-haloketones with $CuCF_3$ has also been contributed by Grushin group [6]. Since the pioneering work reported by MacMillan et al. [7], particularly, the direct radical trifluoromethylation strategy driven by photoredox catalysis under visible-light irradiation has attracted tremendous interests owing to the green and amenable catalytic process [8–10]. However, the high price and strong toxicity of noble photoredox catalysts like polypyridyl iridium and ruthenium complexes [9,10] hinder their practical applications in scale-up synthesis. Additionally, the difficulty associated with the removal of catalyst residue has also led to growing concerns in pharmaceuticals and materials. Therefore, the development of metal-free, heterogeneous methodology to access α-trifluoromethylated ketones under environmentally benign conditions is highly imperative.

Recently, crystalline covalent organic frameworks (COFs) [11–13] have appeared as a new kind of porous materials by integrating functional organic building blocks into predesignable and periodic network architectures using reticular chemistry. Interestingly, the stacked two-dimensional (2D) COFs can form conductive columns, which donates an ideal channel for rapid diffusion and transport of the photogenerated carriers [14]. The initial explorations have proved that 2D-COFs can serve as new platforms for photoinduced water splitting [15–18] and photocatalytic CO_2 reduction [19–21]. Benefiting from the combination of porosity, stability and tailor-made photoactive skeleton, more importantly, a series of imine-based COFs as metal-free heterogeneous photocatalysts for organic synthesis have recently been reported, and they exhibited remarkable activity and recyclability

* Corresponding authors.
E-mail addresses: Henkelman@utexas.edu (G. Henkelman), xm_liu@jlu.edu.cn (X. Liu).
[1] These authors contributed equally.

https://doi.org/10.1016/j.apcatb.2022.121335
Received 28 February 2022; Received in revised form 12 March 2022; Accepted 18 March 2022
Available online 23 March 2022

[22–25]. However, the type of organic reaction driven by COF-based photocatalysts has rarely been reported [22–33]. Particularly, COFs induced photosynthesis of α-trifluoromethylated ketone compounds has not been explored so far, even in heterogeneous semiconductor polymers.

In the context, we have successfully prepared novel COF-based photocatalysts for the synthesis of α-trifluoromethylated ketones from aromatic alkenes and Langlois reagent, which are rich and inexpensive commercial feedstocks. Two electronic donor-acceptor (D-A) type COFs, which possess photoactive benzotrithiophene [34] and triphenyltriazine [35] as electron-donor and electron-acceptor motifs, were constructed based on the imine-linkage and amide linkage, respectively. The D-A structure feature can broaden visible-light harvesting and improve the charge separation efficiency, thus lead to the increasing photocatalytic activity of COFs [24–26]. Because of the stubborn and irreversible character of amide bond, furthermore, the amide-linked DA-COF can own an outstanding chemical stability even under the light system.

2. Experimental section

2.1. Materials

4-aminobenzonitrile, 1,3,5-trichlorobenzene and p-dithiane-2,5-diol were obtained from Chembee Chemical Reagent. Trifluoromethanesulfonic acid, sodium chlorite (80% purity) and sodium trifluoromethanesulfinate (92% purity) were obtained from J&K Scientific. Aluminum chloride and 2-methyl-2-butene were obtained from Aladdin Chemical Reagent. All alkenes were obtained from Energy Chemical Reagent. Other organic solvents for reactions were distilled over appropriate drying reagents under nitrogen. Deuterated solvents for NMR measurement were obtained from Aladdin.

2.2. Synthesis of COF-JLU32

To a mixture of 1,3,5-tris-(4-aminophenyl)triazine (TAPT, 21.2 mg, 0.06 mmol) and benzo[1,2-b:3,4-b':5,6-b'']trithiophene-2,5,8-tricarbaldehyde (BTT, 19.8 mg, 0.06 mmol) was added *o*-dichlorobenzene (3 mL) and HOAc (6 M, 0.3 mL), which was degassed three times. After flame-sealing, the mixture was heated at 120 °C for 72 h. A pale brown powder was collected by centrifugation, washed with tetrahydrofuran (THF, 3 × 5 mL) and acetone (3 × 5 mL). The solid was gathered and dried at 100 °C in vacuum to produce COF-JLU32 with 84% isolated yield.

2.3. Synthesis of COF-JLU33

To a mixture of COF-JLU32 (25.2 mg, 0.12 mmol by imine), 2-methyl-2-butene (1.27 mL, 12.0 mmol, 100 equiv) and dioxane (2.0 mL) was added aqueous $NaClO_2$ solution (0.2 mL, 3.3 M, 0.66 mmol, 5.5 equiv) and glacial acetic acid (68.8 μL, 0.6 mmol, 10 equiv) in sequence. After the suspension was let stand without stirring at room temperature in the dark for 24 h, another aqueous $NaClO_2$ solution (0.2 mL, 3.3 M, 0.66 mmol, 5.5 equiv) was added. After another 24 h, a brown powder was collected by filtration, washed with water (20 mL), 10% sodium thiosulfate solution (20 mL), water (20 mL) and acetone (40 mL) in sequence. The solid was gathered and dried at 100 °C in vacuum to produce COF-JLU33 with 94% isolated yield.

2.4. Characterization

The Fourier transform infrared (FT-IR) spectroscopy were recorded on an Avatar FT-IR 360 spectrometer by using KBr pellets within the wavenumber range 400–4000 cm^{-1}. The liquid NMR spectroscopy were measured by an Avance III-400 NMR spectrometer, and the chemical shift (δ, ppm) is measured with the residual protons of the solvent as the standard. The solid-state ^{13}C CP/MAS NMR spectra were recorded on a Bruker AVANCE III 400 WB spectrometer with a CP contact time of 2 ms and a MAS rate of 5 kHz. The elemental analysis measurement was carried out on an Elementar model vario EL cube analyzer. The UV-Vis absorption spectrum was recorded from 200 to 800 nm on a Shimadzu Corporation U-4100 Spectrophotometer. The field-emission scanning electron microscopy (FE-SEM) was carried out on a JSM - 7900 F microscope. Transmission electron microscopy (TEM) was performed on a JEM-2100 F microscope. The powder X-ray diffraction (PXRD) data were carried out on a PANalytical BV Empyrean diffractometer, the powder was deposited on glass substrate with 2θ range of 1.5–45° at 298 K. The thermogravimetric analysis (TGA) spectrum was recorded from 20 °C to 800 °C on a TA Q500 thermogravimeter at a rate of 10 °C min^{-1} under nitrogen. The catalytic products were quantified by GC analysis (Shimadzu GC-2014 C) using an SE-54 column (30 m × 0.25 mm × 0.25 mm). The Brunauer-Emmett-Teller (BET) method was utilized to calculate the specific surface areas and pore volume on a 3Flex analyzer at 77 K, the polymer was dried in vacuum at 80 °C for more than 6 h before measurement. The nonlocal density functional theory (NLDFT) method was applied for the estimation of pore size distribution. The electron paramagnetic resonance (EPR) spectra were measured by a JEOL JES-FA200 EPR spectrometer. The date of 5,5-dimethyl-1-pyrroline-N-oxide (DMPO) and 2,2,6,6-tetramethylpiperiding (TMP) solution with the concentration of 0.1 M were collected on the measurement parameters, scanning frequency: 9050 MHz; scanning power, 5 mW; central field, 323 mT; scanning width, 100 G; scanning temperature: 298 K.

2.5. Photosynthesis of α-trifluoromethylated ketones

The COF-JLU33 (2.0 mg), alkenes (0.20 mmol), CF_3SO_2Na (0.4 mmol) were added into 0.75 mL dry CH_3OH and 0.25 mL anhydrous acetone. The mixture was stirred in air under irradiation with a green LED lamp (520 nm, 30 W, distance app. 12.0 cm) at room temperature. After the consumption of alkenes, the mixture was filtrated and dried to determine the NMR yield with 1,1,2,2-tetrachloroethane as an internal standard or purified to get the isolated yield by column chromatography on a silica gel column.

2.6. Recycle experiment

In a single recycle experiment, the COF-JLU33 (20 mg), styrene (2.0 mmol), CF_3SO_2Na (4.0 mmol) were added into 7.5 mL dry CH_3OH and 2.5 mL anhydrous acetone. The mixture was stirred in air under irradiation with a green LED lamp (520 nm, 30 W, distance app. 12.0 cm) at room temperature for 10 h. After the first run catalysis was completed, the photocatalyst COF-JLU33 was recycled by centrifugation, then washed with water and THF repeatedly to remove products and unreacted substrates. The yield and conversion were determined by gas chromatography (diphenyl as internal standard). And the recovered COF-JLU33 was dried under vacuum and reused in next cycle in identical conditions.

3. Results and discussion

3.1. Synthesis and characterization of COF-JLUs

An imine-linked DA-COF, named COF-JLU32, was first synthesized by the condensation of 2,4,6-tris(4-aminophenyl)− 1,3,5-triazine and benzo[1,2-b:3,4-b′:5,6-b′′]trithiophene-2,5,8-tricarbaldehyde in *o*-dichlorobenzene (*o*-DCB) and acetic acid (HOAc, 6 M) at 120 °C for 72 h (Scheme 1). The Fourier transform infrared (FT-IR) spectra of COF-JLU32 and corresponding monomers revealed almost disappearance of C═O vibration band at 1676 cm^{-1} and the characteristic absorption of amino group (3200–3400 cm^{-1}) for the co-monomers, and appearance of a new signal at 1618 cm^{-1} assigning to C═N stretching band, which indicated the formation of imine-linkage and the completeness of

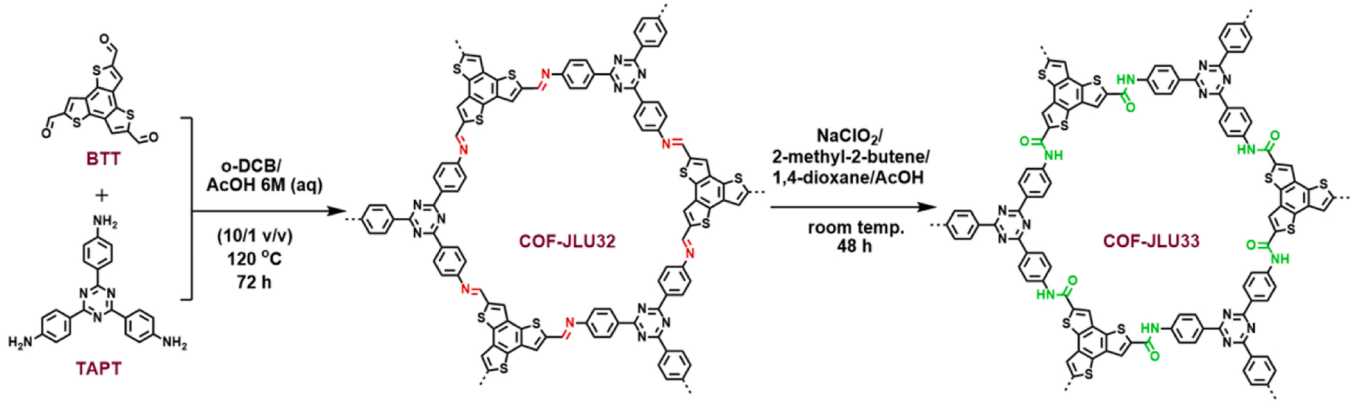

Scheme 1. Synthetic route of COF-JLU32 and COF-JLU33.

concentration reaction. For its small molecule model compound, the similar changes were still found (Fig. 1a, blue line). Additionally, the chemical structure of COF-JLU32 was verified by solid-state ^{13}C cross-polarization magic angle spinning (CP/MAS) nuclear magnetic resonance (NMR) spectroscopy at molecular level. As showed in Fig. 1b, the low-field signal at ~167.1 ppm can be assigned to the carbon of triazine ring. The characteristic carbon signal of imine group for COF-JLU32 was observed at about 151.4 ppm, and the relatively high peak intensity is due to its coincidence with the position of benzene ring carbon bonded with nitrogen. Using the imine linked COF-JLU32 as a precursor, an amine-linked COF (COF-JLU33) was successfully prepared by the reported post-synthetic oxidation strategy (Fig. 1a) [36,37]. Successful conversion of the imine-linked COF-JLU32 to the amide-linked COF-JLU33 was also proved by FT-IR and solid-state ^{13}C CP/MAS NMR methods. FT-IR spectrum of COF-JLU33 showed a new characteristic signal of C═O in the amide group at 1656 cm^{-1} (Fig. 1a, orange line). Compared to COF-JLU32, more importantly, a new peak at about 157.6 ppm assigning to the carbon of amide carbonyl was still gained in the ^{13}C CP/MAS NMR spectrum of COF-JLU33 (Fig. 1b, blue line), at the same time the signal strength at about 151.4 decreased significantly, which clearly indicated the effective conversion from the imine bond into the amide bond.

The permanent porosity of both COF-JLUs was evaluated by utilizing the nitrogen sorption experiment at 77 K. As illustrated in Fig. 2a, the sorption patterns of COF-JLU32 and COF-JLU33 showed the type I reversible sorption isotherms demonstrated by a speed uptake under a low relative pressure, which implying their microporous character. The Brunauer-Emmett-Teller (BET) surface area was calculated to be 1501 $m^2\ g^{-1}$ for COF-JLU32 and 1148 $m^2\ g^{-1}$ for COF-JLU33, respectively. And the pore volume was 0.707 and 0.701 $cm^3\ g^{-1}$ at P/P_0 = 0.99, respectively. Additionally, nonlocal density functional theory (NLDFT) indicated that they have almost the same pore size distribution with a dominant pore width at 1.58 nm, which match well with their simulated values (Fig. 2b).

Furthermore, the crystallinities of both obtained COF-JLUs were confirmed by powder X-ray diffraction (PXRD) analysis. As displayed in Fig. 2c and d, COF-JLU32 and COF-JLU33 displayed the excellent crystallinities. In particular, COF-JLU33 is still highly crystalline after the oxidation reaction. The experimental PXRD curve of COF-JLU32 revealed the obvious diffraction peaks at 4.68°, 8.10°, 9.37°, 12.48° and 25.29°, which assigned to the reflections from (100), (200), (210), (220) and (001) planes of the hexagonal lattice, respectively (Fig. 2c). Compared with the imine-linked COF-JLU32, no evident move of the reflection signals in PXRD pattern of COF-JLU33 was found after the

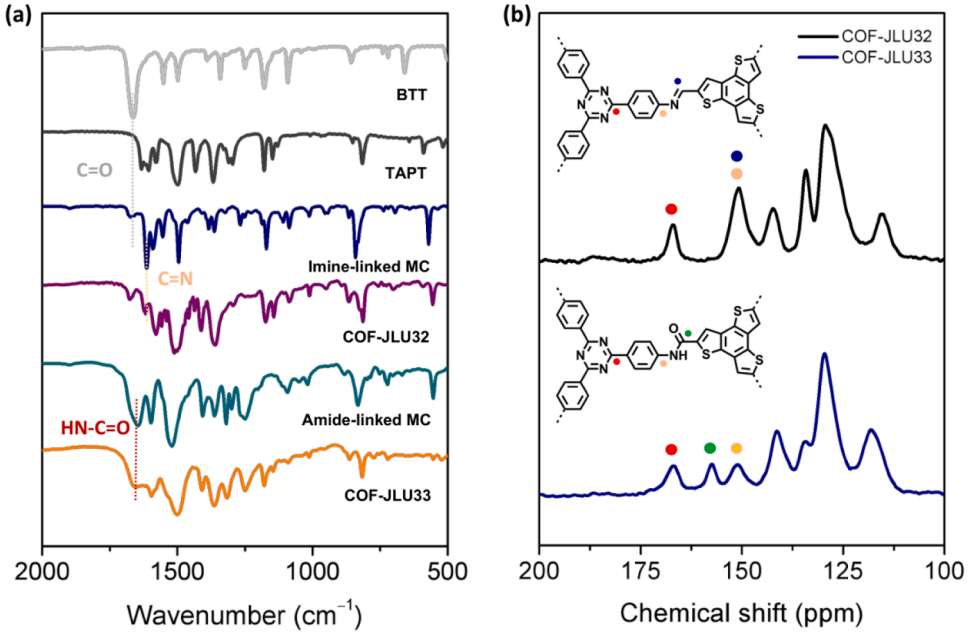

Fig. 1. (a) FT-IR spectra of monomers, model compounds and COF-JLUs. (b) Solid state ^{13}C CP/MAS NMR spectra of COF-JLU32 and COF-JLU33.

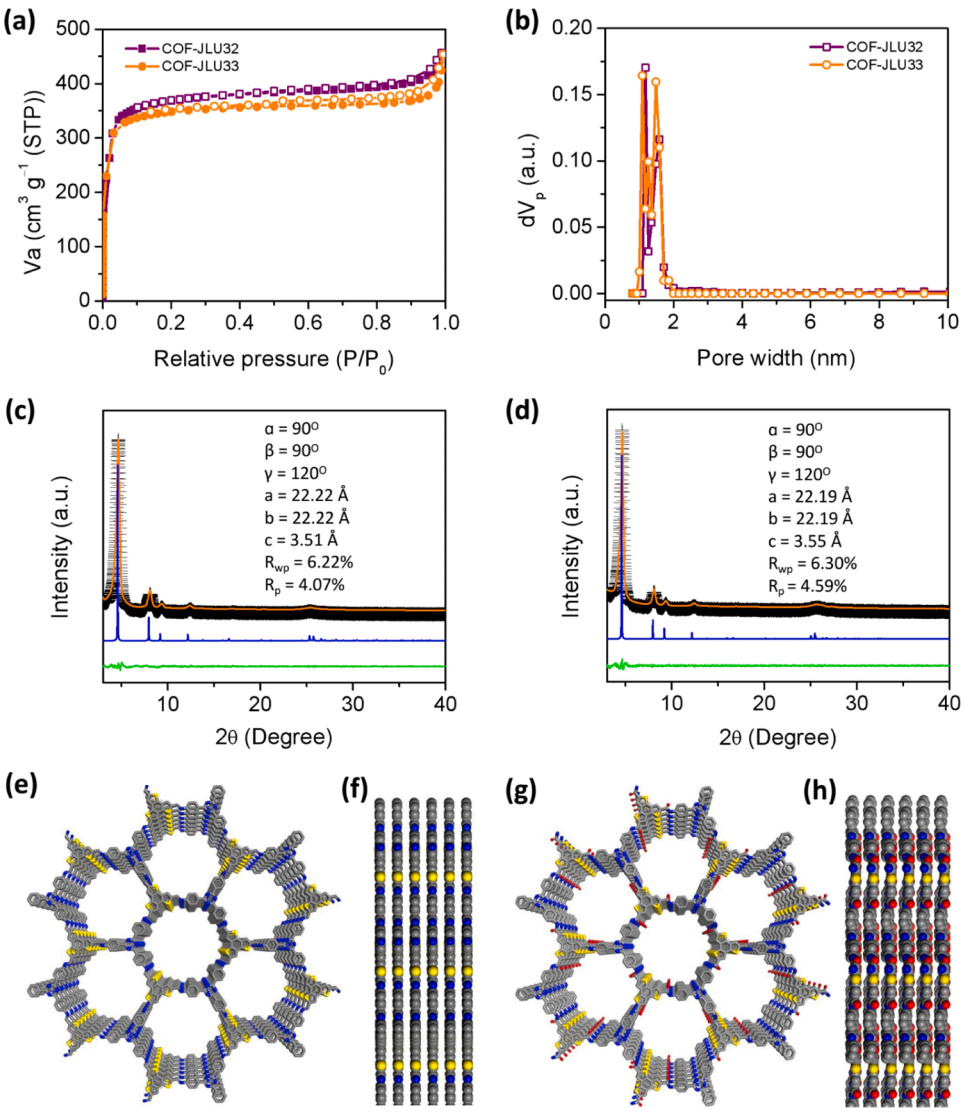

Fig. 2. (a) Nitrogen adsorption (point) and desorption (circle) isotherms of COF-JLUs at 77 K. (b) Pore size distribution of COF-JLUs on the N_2 adsorption isotherm. PXRD profiles of (c) COF-JLU32 and (d) COF-JLU33: Observed PXRD pattern (black line), the Pawley refined pattern (orange line), the simulated pattern (blue) for the AA-stacking model, and the difference plot (green line). (e) Top views and (f) side views of COF-JLU32, (g) Top views and (h) side views of COF-JLU33 (yellow, sulfur; blue, nitrogen; red, oxygen; gray, carbon; hydrogen is omitted for clarity).

transformation of linkages (Fig. 2d). For example, a high-intensity peak at about 4.66°, as well as four relatively wide signals at 8.09°, 9.36°, 12.46° and 25.73° corresponding to the (100), (200), (210), (220) and (001) planes was distinctly observed, implying the high long-range order is remained. The theoretical simulation indicated that two frameworks preferably possess the 2D eclipsed stacking model (Fig. 2e-h). The Pawley refinement showed a negligible difference between the simulated and experimentally observed PXRD pattern (R_{wp} = 6.22%, R_p = 4.07% for COF-JLU32; R_{wp} = 6.30%, R_p = 4.59% for COF-JLU33). Meanwhile, field-emission scanning electron microscopy (FE-SEM) images showed that they are pure solid phase materials with same aggregation morphology (Fig. 3a and b). The high-resolution transmission electron microscopy (HR-TEM) of COF-JLUs displayed that they were prepared as highly ordered particles (Fig. 3c and d).

Thermogravimetric analysis (TGA) was performed on the dry samples under a N_2 atmosphere, which demonstrated that both COFs have a highly thermal stability with decomposition temperature up to 640 °C (Fig. S1). Notably, the weight loss at low temperature for COF-JLU33 may be attributed to the adsorbed water in the pores. Additionally, we still studied the chemical stability of two polymer materials. The corresponding COF samples were treated with water, HCl (12 M), NaOH (14 M) and various organic solvents including tetrahydrofuran (THF), *N*, *N*-dimethlformamide (DMF), methanol (MeOH) at room temperature for 3 days. And then samples were separated by centrifugation, washed and dried in vacuum at 120 °C for 6 h. To our delight, all samples also retained the high crystallinity and skeleton connection proved by PXRD patterns (Fig. S2) and FT-IR spectra (Fig. S3), indicating the outstanding durability of both COF-JLUs.

The UV-Vis diffuse reflectance spectra (DRS) give broad harvesting with maximum peaks at 440 nm for COF-JLU32 and 435 nm for COF-JLU33 in the visible region (Fig. 4a), respectively, according with their color (Fig. 4a insets). According to the Tauc plot, the optical band gap energy (E_g) was calculated to be 2.46 eV for COF-JLU32 and 2.37 eV for COF-JLU33, respectively (Fig. 4b). To further evaluate the electronic structures of COF-JLUs, Mott-Schottky measurements were performed at three diverse frequencies to assess the conduction band (CB) potential of materials. The Mott-Schottky plots pointed out the characteristics of *n*-type semiconductors for COF-JLUs, thus their CB positions are approach to the corresponding flat band potential [38]. Consequently, the CB potential of COF-JLU32 and COF-JLU33 were estimated to be − 1.01 and − 1.10 V (vs. SCE), respectively (Fig. 4c and d). Furthermore, their valence band (VB) potentials can be also calculated to be 1.45 and 1.27 V versus SCE, respectively, according to equation $E_{CB} = E_{VB} - E_g$. The corresponding band structure alignments of COF-JLU32 and COF-JLU33 were schematically showed in Fig. 4e. Compared with the redox potentials for Langlois reagent (CF_3SO_2Na, 1.05 V vs. SCE) [39]

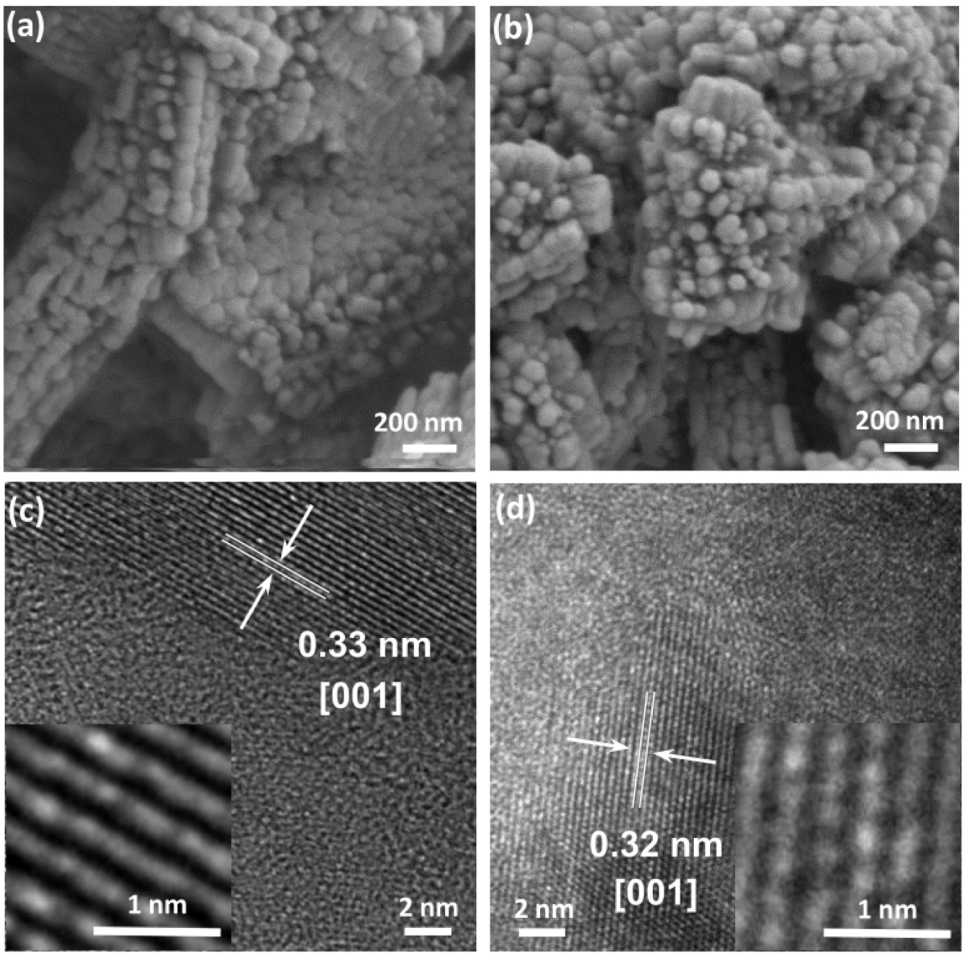

Fig. 3. FE-SEM images of (a) COF-JLU32 and (b) COF-JLU33. HR-TEM images of (c) COF-JLU32 and (d) COF-JLU33.

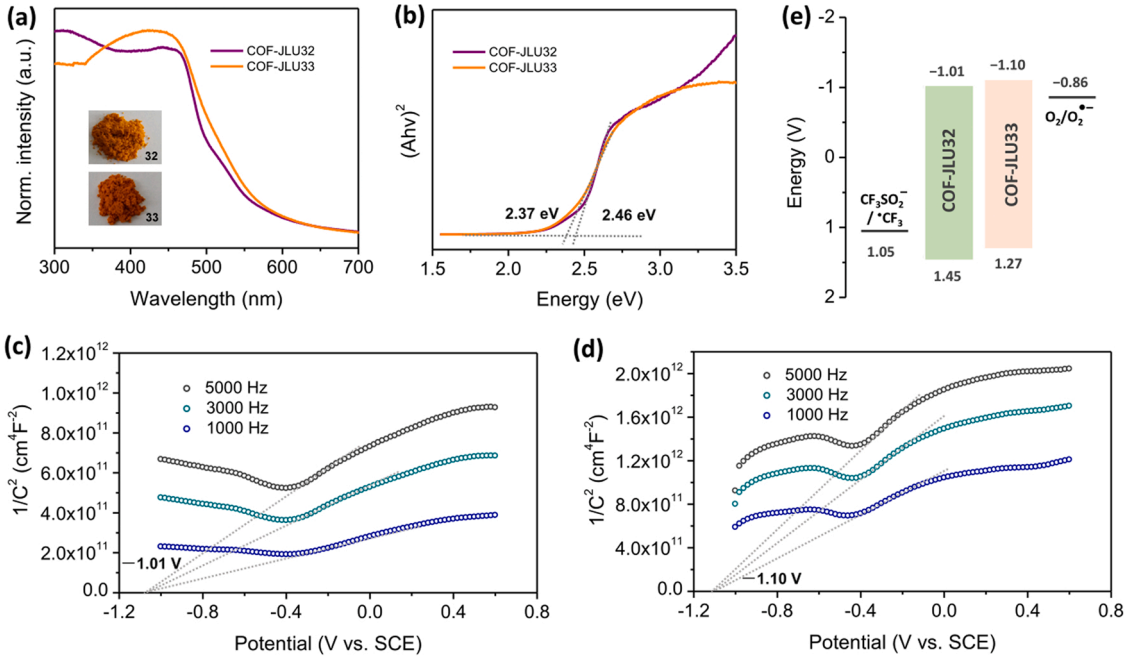

Fig. 4. (a) UV-Vis diffuse reflectance spectra of COF-JLUs. Inset: their optical images. (b) Tauc plots of COF-JLUs. Mott–Schottky plots of (c) COF-JLU32 and (d) COF-JLU33 in 0.1 M Na_2SO_4 aqueous solution at frequency of 1000, 3000 and 5000 Hz. (e) Band structure diagram of COF-JLUs.

oxidation and oxygen reduction (−0.86 V vs. SCE) [40], particularly, the energy levels of both COF-JLUs are well matched.

3.2. Photosynthesis of α-trifluoromethylated ketones by COF-JLUs

Metal-free photosynthesis of α-trifluoromethylated ketones from alkenes with inexpensive CF_3SO_2Na is the most green and sustainable avenue because of the price advantage of reactants and the convenient system. In this context, the new DA-COFs not only have inherent porosity with large surface area, high crystallinity and excellent durability, but also offer broad light response range and appropriate photoredox properties. Therefore, they should be highly promising heterogeneous catalysts for photosynthesis of α-trifluoromethylated ketones. The trifluoromethylation of styrene by COF-JLU33 was first performed as a model example for optimized the reaction conditions. The influences of different solvents on the reaction activity were evaluated. We can find from Table 1, a relative higher yield was realized in acetone (52%) and CH_3OH (58%) compared to CH_3CN (29%) and DMF (26%) (Table 1, entries 1–4). Importantly, the mixed solvent of acetone/CH_3OH can significantly improve the reaction yield (Table 1, entries 5–7). When a mixture of acetone/methanol (v/v = 1/3) as reaction solvent, happily, a high yield of 75% was achieved by COF-JLU33 under visible-light irradiation with a green LED lamp (Table 1, entry 7). Accordingly, an apparent quantum yield (AQY) of 4.91% was obtained, which is comparable to the previously reported polymer-based photocatalysts (Table S1, Entry 1) [41,42]. Further adjusting the amount of photocatalyst and the ratio of styrene to CF_3SO_2Na did not significantly improve the yield (Table 1, Entries 8–10). When white or blue LED lamp was utilized as the light source, relatively poor yields were acquired (Table 1, Entries 11 and 12). In addition, the control experiments demonstrated that photocatalyst, excited light and oxygen gas are essential for photocatalytic trifluoromethylation of styrene (Table 1, Entries 13–15).

Table 1
Photocatalytic α-trifluoromethylated ketones from styrene by COF-JLU[a].

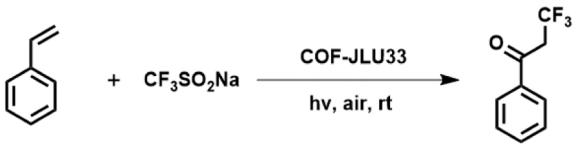

Entry	Catalyst	Solvent	Time (h)	Conv. (%)[b]	Yield (%)[b]
1	COF-JLU33	CH_3CN	10	100	29
2	COF-JLU33	DMF	10	61	26
3	COF-JLU33	Acetone	10	83	52
4	COF-JLU33	MeOH	10	100	58
5	COF-JLU33	Acetone/ MeOH (0.75:0.25)	10	92	69
6	COF-JLU33	Acetone/ MeOH (0.50:0.50)	10	96	71
7	COF-JLU33	Acetone/ MeOH (0.25:0.75)	10	98	75
8[c]	COF-JLU33	Acetone/ MeOH (0.25:0.75)	10	85	66
9[d]	COF-JLU33	Acetone/ MeOH (0.25:0.75)	8	100	76
10[e]	COF-JLU33	Acetone/ MeOH (0.25:0.75)	10	100	72
11[f]	COF-JLU33	Acetone/ MeOH (0.25:0.75)	10	37	23
12[g]	COF-JLU33	Acetone/ MeOH (0.25:0.75)	10	100	65
13	~	Acetone/ MeOH (0.25:0.75)	10	5	0
14[h]	COF-JLU33	Acetone/ MeOH (0.25:0.75)	10	6	0
15[i]	COF-JLU33	Acetone/ MeOH (0.25:0.75)	10	2	0
16	COF-JLU32	Acetone/ MeOH (0.25:0.75)	10	97	71

[a] Reaction conditions: photocatalyst (2.0 mg), styrene (23.0 μL, 0.20 mmol), CF_3SO_2Na (68 mg, 0.40 mmol), anhydrous solvent (1 mL), air, 30 W green LED lamp with 520 nm, 25 °C.
[b] Conversions and yields determined by GC using diphenyl as an internal standard.
[c] COF-JLU33 (1.0 mg).
[d] COF-JLU33 (3.0 mg).
[e] CF_3SO_2Na (0.6 mmol, 3eq).
[f] 8 W white LED lamp.
[g] 30 W blue LED lamp with 460 nm.
[h] In N_2.
[i] Dark.

The generality for photocatalytic synthesis of α-trifluoromethylated ketone compounds over COF-JLU33 was still estimated. As displayed in Table 2, a series of substituted styrenes with electron-withdrawing and electron-donating groups including -CH_3, -^{i}Bu, -OCH_3, -F, -Cl, -Br can be smoothly converted to the corresponding product with good yield of 63–76% (**2b-2i**) under the optimal conditions. For strong electron-withdrawing groups such as -NO_2 and -CN, however, the yield decreased slightly to 59% for **2k** and 53% for **2 l**, even prolonging the reaction time. Significantly, this photocatalytic system was still suitable for the reaction of β-substituted styrenes. And the desired α-trifluoromethylated ketone products were obtained with 40% for **2 m**, 46% for **2 n** and 48% for **2o** yield, respectively. It is noteworthy that the photocatalytic activity of COF-JLU33 is comparable to that of the classical noble metal-based photocatalysts [8].

As a metal-free heterogeneous photocatalyst, more importantly, COF-JLU33 still revealed a superior recyclability. And the COF can be separated rapidly by filtration and reutilized for at least four cycles without noticeable decay of photocatalytic activity (Fig. 5a). Notably, the skeleton connectivity and morphology of COF-JLU33 after photocatalysis were retained (Fig. 5b and d). While its crystallinity and porosity were slightly reduced (Fig. 5c and e), owing to an increase of the disorder structure in the skeleton or the formation of nanosheets [15,43]. In contrast, the imine-linked COF-JLU32 showed a low level of recycling, although it has a similar photocatalytic activity (yield: 71%) compared with COF-JLU33 (Table 1, Entry 16). This is mainly due to the better tolerance of amide-linkages in the skeleton for the catalytic environment [37].

3.3. Photocatalytic mechanism

To gain insights into the photocatalytic mechanism, a series of control experiments were conducted. By adding *N,N*-diisopropylethylamine (DIPEA) as a hole scavenger, a reduced yield of 15% was obtained (Fig. 6a). In addition, the yield of the target product decreased sharply from 75% to 4% in the presence of p-benzoquinone (BQ) as a superoxide radical $O_2^{\bullet-}$ scavenger (Fig. 6a). During the photocatalytic process, on the contrary, 2,2,6,6-tetramethylpiperidine-1-oxyl (TEMPO, a radical scavenger) and sodium azide (NaN_3, a singlet oxygen $^1O_2$ scavenger) as trapping agents were added into the reaction mixture, and almost no products were obtained. These results strongly suggest the existence of holes, radical, $O_2^{\bullet-}$ and $^1O_2$ intermediates during this photocatalysis. The transient photocurrent responses of both COFs indicated efficient photoinduced electron-hole pair separation, and their photocurrent under oxygen atmosphere is lower than that in nitrogen, which could be attributed to the quenching of photogenerated electrons by O_2 to form $O_2^{\bullet-}$ (Fig. 6b). It is well known that photoactive polymer could availably mediate the electron transfer from *N,N,N′,N′*-tetramethyl-p-phenylenediamine (TMPD) to O_2, thus leading to the formation of $O_2^{\bullet-}$ and a blue-colored cationic radical species [44,45]. As expected, the both DA-COFs with high optical activity really provided broad absorption

Table 2
Photosynthesis of α-trifluoromethylated ketones catalyzed by COF-JLU33[a].

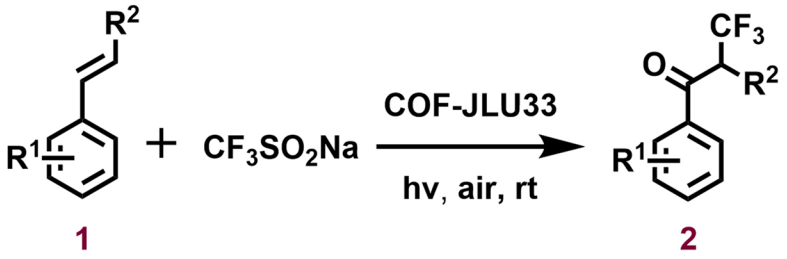

1 2

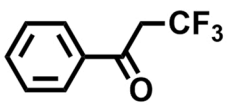

2a
10 h, 75%, 61%

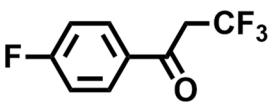

2b
12 h, 63%, 50%

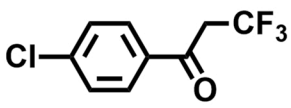

2c
12 h, 67%, 57%

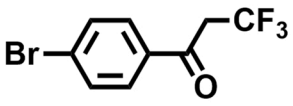

2d
12 h, 68%, 59%

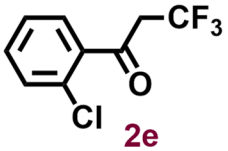

2e
12 h, 68%, 56%

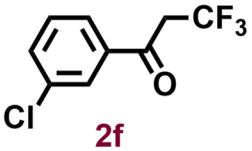

2f
10 h, 70%, 58%

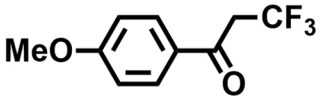

2g
10 h, 76%, 65%

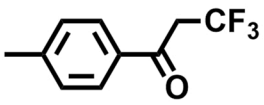

2h
10 h, 76%, 61%

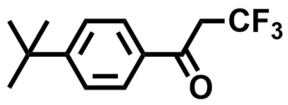

2i
10 h, 74%, 61%

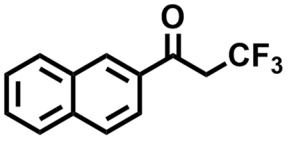

2j
14 h, 66%, 53%

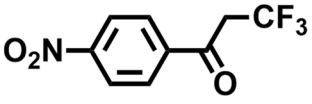

2k
14 h, 59%, 53%

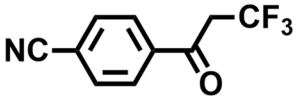

2l
14 h, 53%, 46%

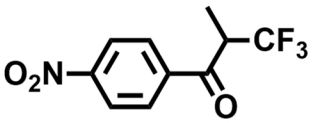

2m
12 h, 40%, 32%

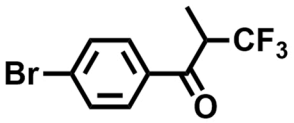

2n
12 h, 46%, 37%

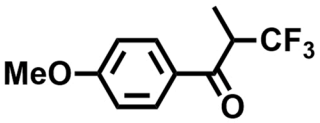

2o
12 h, 48%, 33%

[a]Reaction conditions: COF-JLU33 (2.0 mg), aromatic alkenes (0.20 mmol), CF_3SO_2Na (0.40 mmol), anhydrous acetone/methanol (0.25/0.75 mL), air, 30 W green LED (520 nm), 25 °C. The ^1H NMR yield (black word). The isolated yields (blue word).

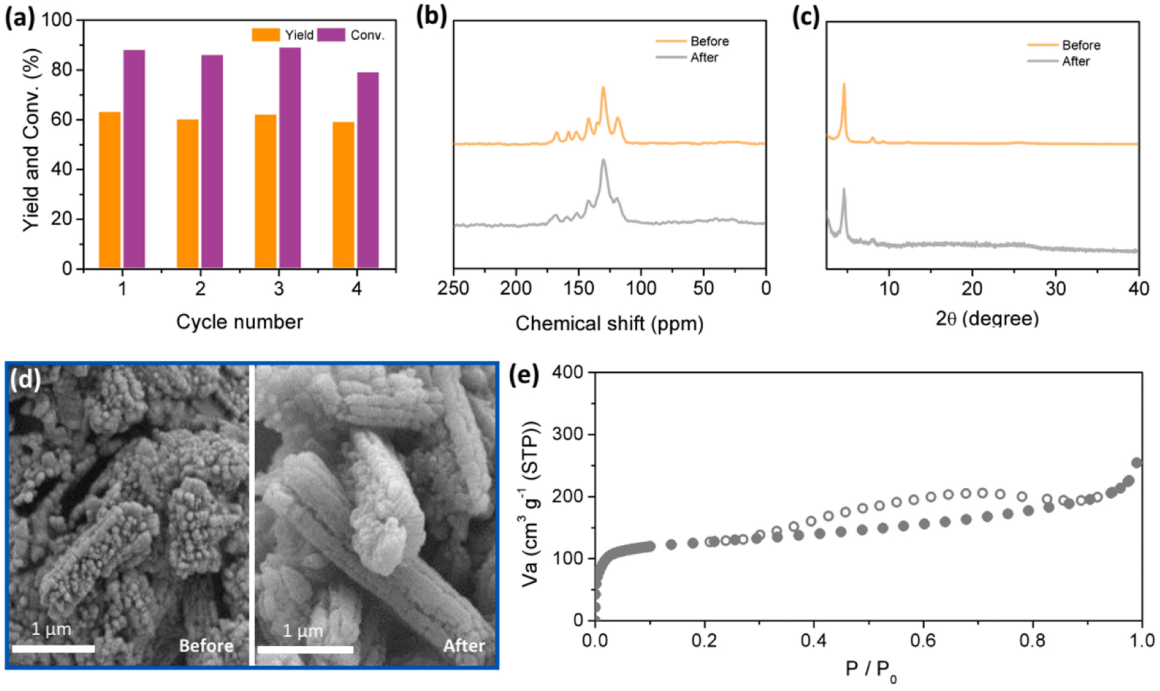

Fig. 5. (a) Reusability of COF-JLU33 for photosynthesis of 2a from styrene. (b) Solid state ^{13}C CP/MAS NMR spectra of COFJLU33 before and after four runs. (c) PXRD curves of COF-JLU33 before and after four runs. (d) SEM images of COF-JLU33 before and after four runs. (e) Nitrogen adsorption (point) and desorption (circle) isotherm of COF-JLU33 after four runs at 77 K. The BET surface area was calculated to be 484.7 $m^2\ g^{-1}$.

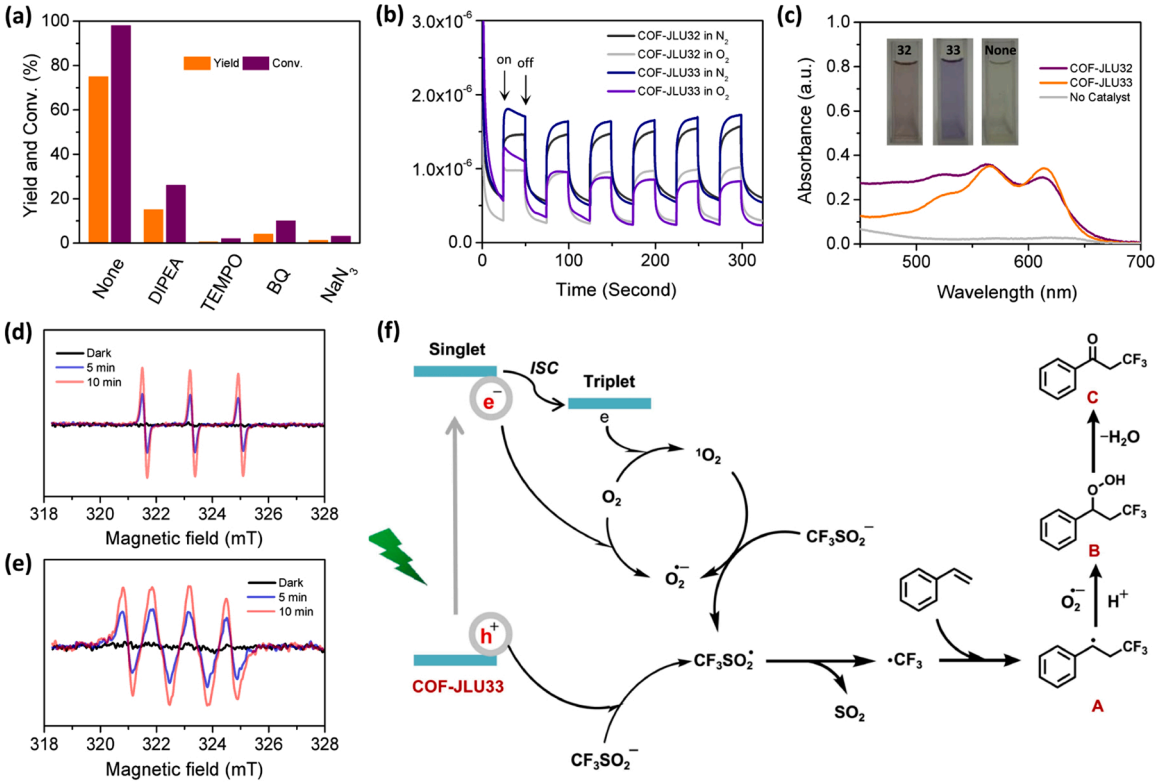

Fig. 6. (a) Influence of scavengers on the photocatalytic yield and conversion of 2a in the control experiments. (b) Photocurrent responses of COF-JLUs in N_2 or O_2 atmosphere. (c) UV-Vis absorption spectra of the TMPD cationic radical generated by COF-JLUs in the presence of oxygen and light. Inset: the photographs. (d) ESR spectra of COF-JLU32 (2.0 mg mL^{-1}) and TMP (0.1 M) in methanol in dark (black line) and under light illumination for 5 min (blue line), 10 min (cyan line). (e) ESR spectra of COF-JLU33 (2.0 mg mL^{-1}) and DMPO (0.1 M) in methanol in dark (black line) and under light illumination for 5 min (blue line), 10 min (cyan line). (f) Proposed mechanism for photocatalytic α-trifluoromethylated ketones from styrene by COF-JLU33.

bands at 566 and 615 nm (Fig. 6c), which demonstrates that the electron transfer process has taken place. Besides, we also investigated the active oxygen species formed by COF-JLU32 and COF-JLU33 through electron paramagnetic resonance (EPR) experiments. Here, 5,5-dimethyl-1-pyrrolin N-oxide (DMPO) and 2,2,6,6-tetramethylpiperidine (TMP) were choosed and used as spin-trapping agents for both active oxygen species $O_2^{\bullet-}$ and $^1O_2$, respectively. As displayed in Fig. 6d and Fig. S4a, we can find that the characteristic signal of the 2,2,6,6-tetramethylpiperidine-1-oxyl (TMPO) nitroxide radical generated from the reaction of $^1O_2$ and TMP was achieved under irradiation of the air-saturated methanol mixture of the COF-JLUs and TMP. When DMPO was used instead of TMP under the same conditions, subsequently, the characteristic peaks attributed to $O_2^{\bullet-}$ were observed clearly under excited light illumination (Fig. 6e and Fig. S4b). These findings indicated that $O_2^{\bullet-}$ and $^1O_2$ were involved in the photosynthesis of α-trifluoromethylated ketone. Based on the observations from the aforementioned results and literature reports [8,46], the reaction mechanism of photosynthesis α-trifluoromethylated ketones was proposed as displayed in Fig. 6 f. Under visible light illumination, the photoactive COF is first excited to form the COF* and generate photoinduced electrons and holes. Two active oxygen species $^1O_2$ and $O_2^{\bullet-}$ were then generated by energy or single electron transfer process from the photogenerated electron to molecular oxygen O_2. The $CF_3SO_2^-$ that ionized from CF_3SO_2Na, converted simultaneously to $CF_3SO_2\bullet$ through electron transfer to the holes and $^1O_2$, then spontaneously producing $\bullet CF_3$, which proved by the trapping test (Fig. S5). The intermediate **A** generated from the radical addition of $\bullet CF_3$ to styrene reacted with $O_2^{\bullet-}$ and combined with proton to get the intermediate **B**. Ultimately, the hydroperoxide intermediate lose a molecule of H_2O and yield the product **C**.

3.4. Expansion of COF-based photocatalysts

Previously, many COF materials were prepared and applied as heterogeneous photocatalysts, and displayed excellent photocatalytic performances [15–31]. Therefore, we choose two types of triazine-based COFs including N_3-COF [47], COF-JLU5 [22], TTA-TTB COF [48] and pyrene-based COFs such as COF-JLU24 [24], COF-JLU25 [24], PyTTA-TPhA-COF [49] as photocatalysts to further explore their catalytic performances for photosynthesis of α-trifluoromethylated ketones. As shown in Table S3, all of the studied triazine-based COFs exhibited better catalytic efficiency than these of pyrene-based COFs, even if the energy level position completely answers the demand (Fig. S6-S8). Consequently, the different photocatalytic activity between the triazine-based COFs and pyrene-based COFs was investigated by density functional theory (DFT) using COF-JLU32 and COF-JLU25 as model materials, respectively. The effective masses of photogenerated electrons and holes for both COFs were calculated through parabolic fitting to the VB and CB (Table 3). A carrier combination index D is defined as the relative effective mass of photogenerated holes to electrons ($D = m_h^*/m_e^*$). It can be clearly found that the D value of COF-JLU32 in these K-path is much larger than that of COF-JLU25 (Table 3), indicating that the triazine-based COF-JLU32 has the better capability to suppresses photogenerated carrier recombination [50,51]. In addition, COF-JLU32 possesses an indirect bandgap by DFT calculation, that can make the recombination of photogenerated carriers more difficult than that of COF-JLU25 with a direct bandgap (Fig. S9) [52]. Furthermore, this proposal can also be confirmed by the composition of the VB and CB in both COFs. The photogenerated electrons generally have lower recombination tendency for the materials with more complex orbital composition. It can be found that two different types of element (S and N) occupy the CB / VB in COF-JLU32, while only one type of elements (C) contributes them for COF-JLU25 in the CB / VB (Fig. S9). In general, the photocatalysis is a very complicated process. From the perspective of electronic structure of materials, the triazine-based COFs can suppress effectively the recombination of photogenerated electron and hole, and produce more intermediate $\bullet CF_3$, resulting in higher catalytic efficiency.

Table 3
The calculated carrier effective masses of the representative pyrene-based COF and triazine-based COF by parabolic fitting to the VB and CB along their specific direction in reciprocal space respectively (accuracy $< 1 \times 10^{-5}$).

Species	COF-JLU25			COF-JLU32		
	G→Y	L_2→G	I→M_2	M→L	H→K	H→A
m_h^*	1.423	0.176	0.425	0.870	19.050	25.893
m_e^*	28.073	0.229	5.879	0.842	1.129	10.045
D	0.051	0.769	0.072	1.033	16.873	2.578

4. Conclusions

In summary, two novel triazine-based DA-COFs were designed and prepared under solvothermal conditions for the photosynthesis of α-trifluoromethylated ketones. They possess broad visible-light absorption, rich redox properties and fast carrier separation efficiency. Significantly, COF-JLU33 as a metal-free photocatalyst not only showed good catalytic activity, which is comparable to the reported homogeneous photocatalytic systems, but also exhibited satisfactory recyclability. DFT results indicated the triazine-based COFs can suppress effectively the recombination of photogenerated carriers, resulting in higher catalytic efficiency. We still highlight that this contribution is the first photosynthesis of α-trifluoromethylated ketones for the heterogeneous organic polymer system, which further extended the application of COFs and promote the development of fluorine chemistry.

Author contributions

X.L. and H.X. conceived the project, designed experiments and provided funding. Z.L. conducted the experiments and analyzed the data. S. M., Z.Z. and Y.Z. provided experimental testing support and gave useful help during the experiments. J.W., G.H. and F.Z. performed the theoretical calculated data and analyzed the results. X.L., Z.L. and G.H. wrote the manuscript and discussed the results with all authors. All data are reported in the main text and supplementary materials.

CRediT authorship contribution statement

Ziping Li: Investigation, Data curation, Formal analysis, Writing – review & editing. **Jia-ao Wang**: Software, Formal analysis, Writing – review & editing. **Si Ma**: Investigation. **Zhenwei Zhang**: Investigation. **Yongfeng Zhi**: Resources. **Fuchun Zhang**: Resources. **Hong Xia**: Project administration, Funding acquisition. **Graeme Henkelman**: Methodology, Writing – review & editing. **Xiaoming Liu**: Conceptualization, Writing – original draft, Supervision, Funding acquisition.

Declaration of Competing Interest

The authors declare that they have no conflict-of-interest statement about the work in this paper.

Acknowledgments

This work was supported by the Natural Science Foundation of China (52073119, 21774040 and 62075081).

Appendix A. Supporting information

Supplementary data associated with this article can be found in the online version at doi:10.1016/j.apcatb.2022.121335.

References

[1] Y. Zhou, J. Wang, Z. Gu, S. Wang, W. Zhu, J.L. Aceña, V.A. Soloshonok, K. Izawa, H. Liu, Next generation of fluorine-containing pharmaceuticals, compounds currently in phase II–III clinical trials of major pharmaceutical companies: new

structural trends and therapeutic areas, Chem. Rev. 116 (2016) 422–518, https://doi.org/10.1021/acs.chemrev.5b00392.
[2] M. Schlosser, CF_3-bearing aromatic and heterocyclic building blocks, Angew. Chem. Int. Ed. 45 (2006) 5432–5446, https://doi.org/10.1002/anie.200600449.
[3] G.K.S. Prakash, A.K. Yudin, Perfluoroalkylation with organosilicon reagents, Chem. Rev. 97 (1997) 757–786, https://doi.org/10.1021/cr9408991.
[4] C.P. Zhang, Z.L. Wang, Q.Y. Chen, C.T. Zhang, Y.C. Gu, J.C. Xiao, Generation of the CF_3 radical from trifluoromethylsulfonium triflate and its trifluoromethylation of styrenes, Chem. Commun. 47 (2011) 6632–6634, https://doi.org/10.1039/C1CC11765C.
[5] T. Kawamoto, R. Sasaki, A. Kamimura, Synthesis of α-trifluoromethylated ketones from vinyl triflates in the absence of external trifluoromethyl sources, Angew. Chem. Int. Ed. 56 (2017) 1342–1345, https://doi.org/10.1002/anie.201608591.
[6] P. Novak, A. Lishchynskyi, V.V. Grushin, Trifluoromethylation of α-haloketones, J. Am. Chem. Soc. 134 (2012) 16167–16170, https://doi.org/10.1021/ja307783w.
[7] P.V. Pham, D.A. Nagib, D.W.C. MacMillan, Photoredox catalysis: a mild, operationally simple approach to the synthesis of α-trifluoromethyl carbonyl compounds, Angew. Chem. Int. Ed. 50 (2011) 6119–6122, https://doi.org/10.1002/anie.201101861.
[8] R. Tomita, Y. Yasu, T. Koike, M. Akita, Combining photoredox-catalyzed trifluoromethylation and oxidation with DMSO: facile synthesis of α-trifluoromethylated ketones from aromatic alkenes, Angew. Chem. Int. Ed. 53 (2014) 7144–7148, https://doi.org/10.1002/anie.201403590.
[9] S. Das, A.S.K. Hashmi, T. Schaub, Direct photoassisted α-trifluoromethylation of aromatic ketones with trifluoroacetic anhydride (TFAA), Adv. Synth. Catal. 361 (2019) 720–724, https://doi.org/10.1002/adsc.201801305.
[10] S. Liu, J. Jie, J. Yu, X. Yang, Visible light induced trifluoromethyl migration: easy access to α-trifluoromethylated ketones from enol triflates, Adv. Synth. Catal. 360 (2018) 267–271, https://doi.org/10.1002/adsc.201701051.
[11] K. Geng, T. He, R. Liu, S. Dalapati, K.T. Tan, Z. Li, S. Tao, Y. Gong, Q. Jiang, D. Jiang, Covalent organic frameworks: design, synthesis, and functions, Chem. Rev. 120 (2020) 8814–8933, https://doi.org/10.1021/acs.chemrev.9b00550.
[12] J.L. Segura, M.J. Mancheno, F. Zamora, Covalent organic frameworks based on Schiff-base chemistry: synthesis, properties and potential applications, Chem. Soc. Rev. 45 (2016) 5635–5671, https://doi.org/10.1039/C5CS00878F.
[13] Y.P. Song, Q. Sun, B. Aguila, S.Q. Ma, Opportunities of covalent organic frameworks for advanced applications, Adv. Sci. 6 (2019) 1801410, https://doi.org/10.1002/advs.201801410.
[14] M.S. Lohse, T. Bein, Covalent organic frameworks: structures, synthesis, and applications, Adv. Funct. Mater. 28 (2018) 1705553, https://doi.org/10.1002/adfm.201705553.
[15] L. Stegbauer, K. Schwinghammer, B.V. Lotsch, A hydrazone-based covalent organic framework for photocatalytic hydrogen production, Chem. Sci. 5 (2014) 2789–2793. ⟨https://doi.org/10.1039/C4SC00016A⟩.
[16] X. Wang, L. Chen, S.Y. Chong, M.A. Little, Y. Wu, W.H. Zhu, R. Clowes, Y. Yan, M. A. Zwijnenburg, R.S. Sprick, A.I. Cooper, Sulfone-containing covalent organic frameworks for photocatalytic hydrogen evolution from water, Nat. Chem. 10 (2018) 1180–1189, https://doi.org/10.1038/s41557-018-0141-5.
[17] E. Jin, Z. Lan, Q. Jiang, K. Geng, G. Li, X. Wang, D. Jiang, 2D sp^2 carbon-conjugated covalent organic frameworks for photocatalytic hydrogen production from water, Chem 5 (2019) 1632–1647, https://doi.org/10.1016/j.chempr.2019.04.015.
[18] W. Chen, L. Wang, D. Mo, F. He, Z. Wen, X. Wu, H. Xu, L. Chen, Modulating benzothiadiazole-based covalent organic frameworks via halogenation for enhanced photocatalytic water splitting, Angew. Chem. Int. Ed. 59 (2020) 16902–16909, https://doi.org/10.1002/anie.202006925.
[19] W. Zhong, R. Sa, L. Li, Y. He, L. Li, J. Bi, Z. Zhuang, Y. Yu, Z. Zou, A covalent organic framework bearing single Ni sites as a synergistic photocatalyst for selective photoreduction of CO_2 to CO, J. Am. Chem. Soc. 141 (2019) 7615–7621, https://doi.org/10.1021/jacs.9b02997.
[20] Z. Fu, X. Wang, A.M. Gardner, X. Wang, S.Y. Chong, G. Neri, A.J. Cowan, L. Liu, X. Li, A. Vogel, R. Clowes, M. Bilton, L. Chen, R.S. Sprick, A.I. Cooper, A stable covalent organic framework for photocatalytic carbon dioxide reduction, Chem. Sci. 11 (2020) 543–550, https://doi.org/10.1039/C9SC03800K.
[21] M.P. Kou, W. Liu, Y.Y. Wang, J.D. Huang, Y.L. Chen, Y. Zhou, Y. Chen, M.Z. Ma, K. Lei, P.K. Wong, L.Q. Ye, Photocatalytic CO_2 conversion over single-atom MoN_2 sites of covalent organic framework, Appl. Catal. B Environ. 291 (2021), 120146, https://doi.org/10.1016/j.apcatb.2021.120146.
[22] Y. Zhi, Z. Li, X. Feng, H. Xia, Y. Zhang, Z. Shi, Y. Mu, X. Liu, Covalent organic frameworks as metal-free heterogeneous photocatalysts for organic transformations, J. Mater. Chem. A Mater. Energy Sustain. 5 (2017) 22933–22938, https://doi.org/10.1039/C7TA07691F.
[23] Z. Li, Y. Zhi, P. Shao, H. Xia, G. Li, X. Feng, X. Chen, Z. Shi, X. Liu, Covalent organic framework as an efficient, metal-free, heterogeneous photocatalyst for organic transformations under visible light, Appl. Catal. B Environ. 245 (2019) 334–342, https://doi.org/10.1016/j.apcatb.2018.12.065.
[24] Z. Li, S. Han, C. Li, P. Shao, H. Xia, H. Li, X. Chen, X. Feng, X. Liu, Screening metal-free photocatalysts from isomorphic covalent organic frameworks for the C-3 functionalization of indoles, J. Mater. Chem. A Mater. Energy Sustain. 8 (2020) 8706–8715, https://doi.org/10.1039/D0TA02164D.
[25] Z. Zhang, J. Jia, Y. Zhi, S. Ma, X. Liu, Porous organic polymers for light-driven organic transformations, Chem. Soc. Rev. (Advance Article) (2022), https://doi.org/10.1039/D1CS00808K.
[26] S. Li, L. Li, Y. Li, L. Dai, C. Liu, Y. Liu, J. Li, J. Lv, P. Li, B. Wang, Fully conjugated donor-acceptor covalent organic frameworks for photocatalytic oxidative amine coupling and thioamide cyclization, ACS Catal. 10 (2020) 8717–8726, https://doi.org/10.1021/acscatal.0c01242.
[27] S. Bi, P. Thiruvengadam, S. Wei, W. Zhang, F. Zhang, L. Gao, J. Xu, D. Wu, J. S. Chen, F. Zhang, Vinylene-bridged two-dimensional covalent organic frameworks via Knoevenagel condensation of tricyanomesitylene, J. Am. Chem. Soc. 142 (2020) 11893–11900, https://doi.org/10.1021/jacs.0c04594.
[28] X. Lia, S.X. Yang, F.L. Zhang, L.Y. Zheng, X.J. Lang, Facile synthesis of 2D covalent organic frameworks for cooperative photocatalysis with TEMPO: the selective aerobic oxidation of benzyl amines, Appl. Catal. B Environ. 303 (2022), 120846, https://doi.org/10.1016/j.apcatb.2021.120846.
[29] Y. Meng, Y. Luo, J. Shi, H. Ding, X. Lang, W. Chen, A. Zheng, J. Sun, C. Wang, 2D and 3D porphyrinic covalent organic frameworks: the influence of dimensionality on functionality, Angew. Chem. Int. Ed. 59 (2020) 3624–3629, https://doi.org/10.1002/anie.201913091.
[30] P.F. Wei, M.Z. Qi, Z.P. Wang, S.Y. Ding, W. Yu, Q. Liu, L.K. Wang, H.Z. Wang, W. K. An, W. Wang, Benzoxazole-linked ultrastable covalent organic frameworks for photocatalysis, J. Am. Chem. Soc. 140 (2018) 4623–4631, https://doi.org/10.1021/jacs.8b00571.
[31] S. Liu, W. Pan, S. Wu, X. Bu, S. Xin, J. Yu, H. Xu, X. Yang, Visible-light-induced tandem radical addition-cyclization of 2-Aryl phenyl isocyanides catalysed by recyclable covalent organic frameworks, Green Chem. 21 (2019) 2905–2910, https://doi.org/10.1039/C9GC00022D.
[32] R. Chen, J. Shi, Y. Ma, G. Lin, X. Lang, C. Wang, Designed synthesis of a 2D porphyrin-based sp^2 carbon-conjugated covalent organic framework for heterogeneous photocatalysis, Angew. Chem. Int. Ed. 58 (2019) 6430–6434, https://doi.org/10.1002/anie.201902543.
[33] R. Chen, Y. Wang, Y. Ma, A. Mal, X. Gao, L. Gao, L. Qiao, X.B. Li, L.Z. Wu, C. Wang, Rational design of isostructural 2D porphyrin-based covalent organic frameworks for tunable photocatalytic hydrogen evolution, Nat. Commun. 12 (2021) 1354, https://doi.org/10.1038/s41467-021-21527-3.
[34] H. Wei, J. Ning, X. Cao, X. Li, L. Hao, Benzotrithiophene-based covalent organic frameworks: construction and structure transformation under ionothermal condition, J. Am. Chem. Soc. 140 (2018) 11618–11622, https://doi.org/10.1021/jacs.8b08282.
[35] M. Liu, Q. Huang, S. Wang, Z. Li, B. Li, S. Jin, B. Tan, Crystalline covalent triazine frameworks by insitu oxidation of alcohols to aldehyde monomers, Angew. Chem. Int. Ed. 57 (2018) 11968–11972, https://doi.org/10.1002/anie.201806664.
[36] S. Ma, Z. Li, J. Jia, Z. Zhang, H. Xia, H. Li, X. Chen, Y. Xu, X. Liu, 2D amide-linked covalent organic frameworks as efficient heterogeneous photocatalysts in water, Chin. J. Catal. 42 (2021) 2010–2019, https://doi.org/10.1016/S1872-2067(21)63836-6.
[37] X. Han, J. Huang, C. Yuan, Y. Liu, Y. Cui, Chiral 3D covalent organic frameworks for high performance liquid chromatographic enantioseparation, J. Am. Chem. Soc. 140 (2018) 892–895, https://doi.org/10.1021/jacs.7b12110.
[38] W. Jiang, Q. Ruan, J. Xie, X. Chen, Y. Zhu, J. Tang, Oxygen-doped carbon nitride aerogel: a self-supported photocatalyst for solar-to-chemical energy conversion, Appl. Catal. B Environ. 236 (2018) 428–435, https://doi.org/10.1016/j.apcatb.2018.05.050.
[39] D.J. Wilger, N.J. Gesmundo, D.A. Nicewicz, Catalytic hydrotrifluoromethylation of styrenes and unactivated aliphatic alkenes via an organic photoredox system, Chem. Sci. 4 (2013) 3160–3165, https://doi.org/10.1039/C3SC51209F.
[40] H. Xu, Y. Zhang, X. Lang, TEMPO visible light photocatalysis: the selective aerobic oxidation of thiols to disulfides, Chin. Chem. Lett. 31 (2020) 1520–1524, https://doi.org/10.1016/j.cclet.2019.10.024.
[41] W. Huang, N. Huber, S. Jiang, K. Landfester, K.A.I. Zhang, Covalent triazine framework nanoparticles via size-controllable confinement synthesis for enhanced visible-light photoredox catalysis, Angew. Chem. Int. Ed. 59 (2020) 18368–18373, https://doi.org/10.1002/anie.202007358.
[42] Q. Li, X. Lan, G. An, L. Ricardez-Sandoval, Z. Wang, G. Bai, Visible-light-responsive anthraquinone functionalized covalent organic frameworks for metal-free selective oxidation of sulfides: effects of morphology and structure, ACS Catal. 10 (2020) 6664–6675, https://doi.org/10.1021/acscatal.0c00290.
[43] D.N. Bunck, W.R. Dichtel, Bulk synthesis of exfoliated two-dimensional polymers using hydrazone-linked covalent organic frameworks, J. Am. Chem. Soc. 135 (2013) 14952–14955, https://doi.org/10.1021/ja408243n.
[44] S. Han, Z. Li, S. Ma, Y. Zhi, H. Xia, X. Chen, X. Liu, Bandgap engineering in benzotrithiophene-based conjugated microporous polymers: a strategy for screening metal-free heterogeneous photocatalyts, J. Mater. Chem. A Mater. Energy Sustain. 9 (2021) 3333–3340, https://doi.org/10.1039/D0TA10232F.
[45] Y. Zhi, Z. Yao, W. Jiang, H. Xia, Z. Shi, Y. Mu, X. Liu, Conjugated microporous polymers as heterogeneous photocatalysts for efficient degradation of a mustard-gas simulant, ACS Appl. Mater. Interface 11 (2019) 37578–37585, https://doi.org/10.1021/acsami.9b10958.
[46] L. Zhao, P. Li, H. Zhang, L. Wang, Photoinduced synthesis of α-trifluoromethylated ketones through the oxidative trifluoromethylation of styrenes using CF_3SO_2Na as a trifluoromethyl reagent without an external photoredox catalyst, Org. Chem. Front. 6 (2019) 87–93, https://doi.org/10.1039/C8QO01079J.
[47] V.S. Vyas, F. Haase, L. Stegbauer, G. Savasci, F. Podjaski, C. Ochsenfeld, B. V. Lotsch, Tunable azine covalent organic framework platform for visible light-induced hydrogen generation, Nat. Commun. 6 (2015) 8508, https://doi.org/10.1038/ncomms9508.
[48] P. Wang, Q. Xu, Z. Li, W. Jiang, Q. Jiang, D. Jiang, Exceptional iodine capture in 2D covalent organic frameworks, Adv. Mater. 30 (2018) 1801991, https://doi.org/10.1002/adma.201801991.
[49] N. Huang, P. Wang, M.A. Addicoat, T. Heine, D. Jiang, Ionic covalent organic frameworks: design of a charged interface aligned on 1D channel walls and its unusual electrostatic functions, Angew. Chem. Int. Ed. 56 (2017) 4982–4986, https://doi.org/10.1002/anie.201611542.

[50] W. Yu, D. Xu, T. Peng, Enhanced photocatalytic activity of g-C_3N_4 for selective CO_2 reduction to CH_3OH via facile coupling of ZnO: a direct Z-scheme mechanism, J. Mater. Chem. A Mater. Energy Sustain. 3 (2015) 19936–19947, https://doi.org/10.1039/C5TA05503B.

[51] H. Zhang, L. Liu, Z. Zhou, Towards better photocatalysts: first-principles studies of the alloying effects on the photocatalytic activities of bismuth oxyhalides under visible light, Phys. Chem. Chem. Phys. 14 (2012) 1286–1292, https://doi.org/10.1039/C1CP23516H.

[52] K.L. Zhang, C.M. Liu, F.Q. Huang, C. Zheng, W.D. Wang, Study of the electronic structure and photocatalytic activity of the BiOCl photocatalyst, Appl. Catal. B Environ. 68 (2006) 125–129, https://doi.org/10.1016/j.apcatb.2006.08.002.